Eur. Phys. J. B **51**, 293–300 (2006)
DOI: 10.1140/epjb/e2006-00208-8

THE EUROPEAN PHYSICAL JOURNAL B

Core level spectroscopy and RHEED analysis of $KGd_{0.95}Nd_{0.05}(WO_4)_2$ surface

V.V. Atuchin[1,a], V.G. Kesler[2,b], N.Yu. Maklakova[3,c], L.D. Pokrovsky[1], and D.V. Sheglov[4,d]

[1] Laboratory of Optical Materials and Structures, Institute of Semiconductor Physics, SB RAS, Novosibirsk, 630090, Russia
[2] Technical Centre, Institute of Semiconductor Physics, SB RAS, Novosibirsk, 630090, Russia
[3] Innovation Department, Institute of Geology and Mineralogy, SB RAS, Novosibirsk, 630090, Russia
[4] Laboratory of Electron Microscopy and Submicron Structures, Institute of Semiconductor Physics, SB RAS, Novosibirsk, 630090, Russia

Received 25 October 2005 / Received in final form 12 January 2006
Published online 1st June 2006 –

Abstract. A study of the surface structure and electronic properties of (010) $KGd_{0.95}Nd_{0.05}(WO_4)_2$ (Nd:KGW) using RHEED analysis and XPS is presented. It is shown that Nd doping has a negligible effect on the core levels of the basic elements. A bombardment of the Nd:KGW crystal with 3-keV Ar ions results in surface amorphization accompanied by the generation of tungsten ions in lower valence states.

PACS. 33.60.Fy X-ray photoelectron spectra – 61.66.Fn Inorganic compounds – 82.80.Pv Electron spectroscopy (X-ray photoelectron (XPS), Auger electron spectroscopy (AES), etc.)

1 Introduction

Monoclinic α-$KGd(WO_4)_2$ (KGW) is one of the best host materials for laser active lanthanide RE^{3+}(RE = Pr, Nd, Dy, Ho, Er, Tm, Yb) ions. The isomorphous substitution of RE^{3+} ions for Gd in the KGW lattice is possible for comparatively high doping levels without loss of optical quality of the crystal [1]. Comparative analysis of Nd-doped optical crystals classifies Nd:KGW among most effective mediums for laser generation in the near IR range, because of its very high generation performance at low pump energies [2–5]. It is well known that the KGW crystal has a large cubic optical nonlinearity $\chi^{(3)}$ and can be used as an effective medium in lasers with ultralow threshold stimulated Raman scattering [2,6,7]. Recently, a method was reported for the formation of Nd:KGW optical waveguide layers using a pulsed laser deposition technique that provides the scope for creation of integrated Nd:KGW thin film lasers [8–10]. There is the potential for using light ion implantation technique in fabrication of Nd:KGW optical waveguides [11].

Practical applications of doped KGW crystals in laser systems and integrated optics call for preparation of high quality optical surfaces with as low scattering losses as possible and good chemical stability. At the same time, it is well known that severe modifications of the top surface of oxide crystals happen occasionally due to interaction with complex polishing mixtures. Strong changes in chemical composition and structure are probable during thin film formation by different techniques. Most of the previous works on KGW discussed the structure and spectroscopic properties of bulk RE-doped crystals, while information on other properties of pure and doped KGW is very scarce or absent. The present study aims at observing the electronic and structural properties of Nd:KGW crystal surfaces prepared by polishing. Besides this, the effects of an Ar ion beam on the characteristics of the Nd:KGW top surface will be traced to estimate the potential of ion sputtering for the preparation of fine optical surfaces of the crystal.

2 Experimental

A plate with (010) big plane and dimensions $7 \times 8 \times 1\,mm^3$ was prepared by mechanical polishing in water-based suspension at room temperature. The crystal has intensive lilac color and the Nd doping level was estimated by the supplier as 4 at.%. The crystallographic properties of the Nd:KGW optical surface were evaluated by Reflection high energy electron diffraction (RHEED) at an electron accelerating voltage of 50 kV. For charging effect elimination a charge-neutralization flood gun was used.

[a] e-mail: atuchin@thermo.isp.nsc.ru
[b] e-mail: kesler@isp.nsc.ru
[c] e-mail: n_maklakova@mail.ru
[d] e-mail: sheglov@thermo.isp.nsc.ru

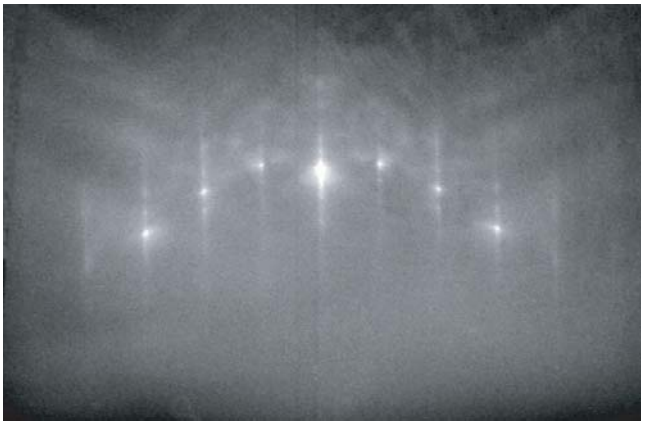

a

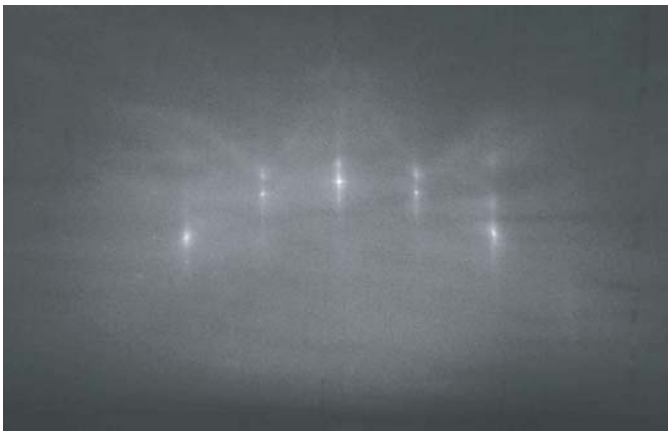

b

Fig. 1. RHEED patterns of the Nd:KGW surface: (a) electron beam is along [100] and (b) electron beam is along [001].

Surface microrelief has been controlled by Atomic force microscopy (AFM) in semi-contact mode.

The electronic parameters and surface element composition were studied with X-ray photoelectron spectroscopy (XPS). X-ray photoemission spectra were recorded with a MAC-2 (Riber) analyzer using nonmonochromatic Mg Kα radiation (1253.6 eV). The energy resolution of the instrument was $\Delta E = 0.5$ eV. Just before an observation of Nd:KGW surface the binding energy scale was calibrated in reference to the Cu $2p$ (932.7 eV) and Cu $3p$ (75.1 eV) lines, yielding an accuracy of ± 0.1 eV in any peak position determination. Using these two reference lines for calibration, one with low and another with high binding energy, is of particular importance for Nd:KGW in which the representative Nd $3d$ and Gd $3d$ core levels appear at very high binding energies. Surface charging effects were taken into account in reference to the C $1s$ level (284.6 eV) of adventitious carbon. To remove surface contaminations, bombardment by Ar^+ ions has been performed with an energy of 3 keV at sample current 100 nA. The ion beam was rastered over an area of 7×20 mm^2 and the sputtering rate was estimated as 0.25 Å/min. Sputtering for 105 min

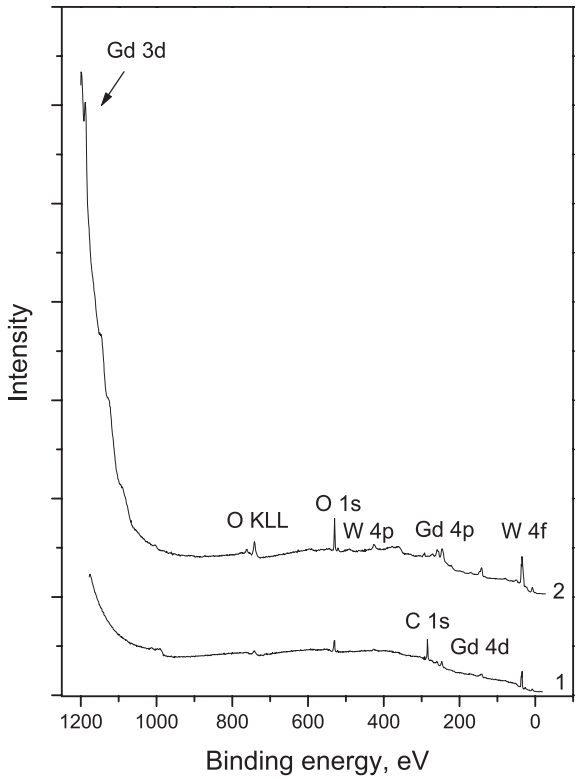

Fig. 2. Survey XPS spectra for (1) initial and (2) clean Nd:KGW surface sputtered for 165 min.

results in complete suppression of the C $1s$ signal. To relate the energy scales for initial and bombarded surfaces, the persistence of binding energies of W $4f_{7/2}$ core level in these spectra is assumed.

3 Electronic structure

In Figure 1 the RHEED patterns are shown for polished and chemically cleaned Nd:KGW surface. The angle between azimuths of the patterns (a) and (b) was 95°, in close relation with an angle 94.4° between [100] and [001] axes in pure KGW, C2/c [4]. The patterns show the combination of monocrystal streaks superimposed with wide Kikuchi lines. The crystallographic parameters of the crystal surface were very close to those inherent to (010) KGW. Thus, the only crystal phase detected on the plate surface was identified as Nd:KGW.

In Figure 2 the survey XPS spectra recorded for the initial and sputtered plate surface are shown. The spectrum (1) related to the initial surface displays the presence of the most intensive lines of KGW constituent elements and a strong C $1s$ core level related seemingly to hydrocarbon contaminations applied in RHEED chamber. The signal of the C $1s$ line was completely suppressed after 105 min of surface bombardment by Ar^+ ions. The spectrum (2) recorded after prolonged sputtering shows a very complex photoelectron spectrum of KGW with numerous peak superposition and fine structure due to the

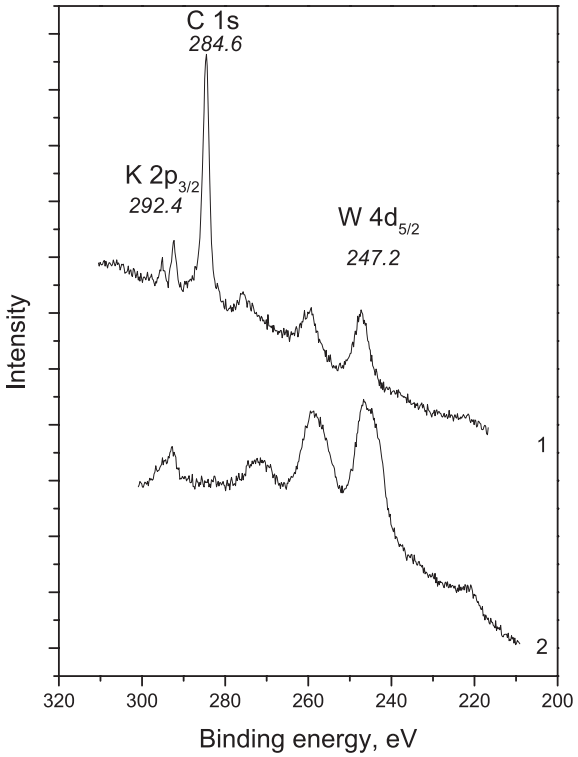

Fig. 3. Binding energy range of K 2*p*–C 1*s*–W 4*d* core levels for (1) initial Nd:KGW surface and (2) surface sputtered for 165 min.

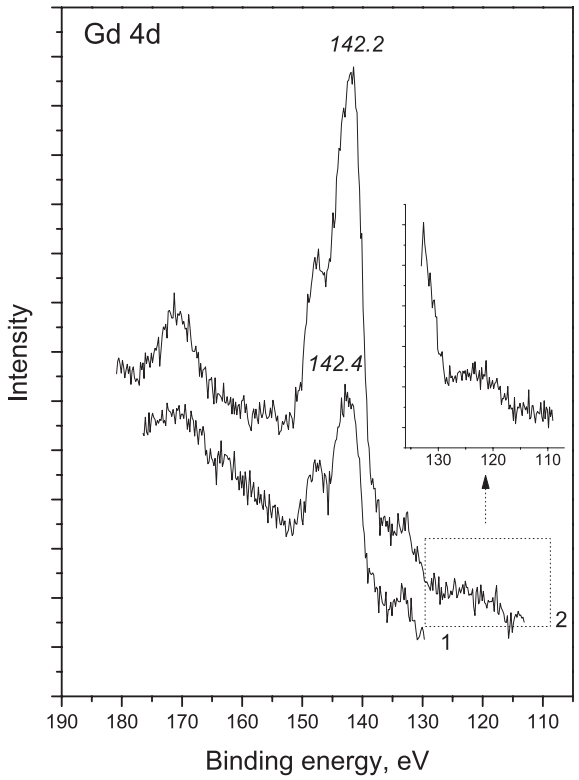

Fig. 4. Detailed spectra of Gd 4*d* core level for (1) initial and (2) bombarded surfaces.

large number of Gd and W core levels. All spectral features measured for initial and bombarded surfaces were attributed to basic elements K, Nd, Gd, W and O. The only exception is a weak line at 1013.7 eV, detected for the initial surface.

In Figure 3 the binding energy range of K 2*p*–C 1*s*–W 4*d* core levels is presented. The spectrum of the initial surface displays an intensive C 1*s* core level with a satellite at ∼276.2 eV excited by K$\alpha_{3,4}$ components of X-ray radiation. Contrary to that, the surface cleaned by Ar^+ bombardment is free of carbon contaminations. Besides this, as a result of interaction of Ar^+ ions with crystal surface new features appear in K 2*p* and W 4*d* doublets. So, clearly the K 2*p* doublet found for the initial surface transforms into a continuous band because of the appearance of new K $2p_{1/2}$ and K $2p_{3/2}$ spectral components, seemingly due to the generation of new K^+ ion states with different chemical environments. Earlier, a similar effect has been detected for another potassium containing crystal, $KTiOPO_4$ (KTP) [12]. It should be noted that the binding energy of the maximum of the K 2*p* band for the bombarded surface and the binding energy of the more intense K $2p_{3/2}$ line for the initial surface are the same. Thus, the dominant part of K^+ ions in the bombarded layer has the same chemical environment as in the initial Nd:KGW crystal lattice. As for the W 4*d* doublet, broadening of both W $4d_{5/2}$ and W $4d_{3/2}$ lines is evident for the bombarded surface owing to the formation of new intensive components on the lower energy side of the lines. In parallel, the broadening has been also detected for other tungsten core levels W 4*f* and W 4*p*. The transformation of the W 4*f* doublet has been discussed in the literature for several tungstates subjected to Ar^+ bombardment and was attributed to partial transition of tungsten ions from W^{6+} state to lower valence states due to oxygen loss from the top surface layers [13–16].

The Gd 4*d* core level is presented in Figure 4. Only a slight shift in the binding energy position of the Gd $4d_{5/2}$ peak has been induced by surface bombardment. The binding energy of the maximum of the Gd $4d_{5/2}$ peak is in good agreement with the values measured earlier for several gadolinium containing oxides, Gd_2O_3 (142.50 eV, C 1*s* line at 284.6 eV)) [17] and $Gd(OH)_3$ (142.3 eV, C 1*s* line at 285.0 eV) [18]. However, a comparatively low binding energy of the Gd $4d_{5/2}$ core level was found in $GdNbO_4$ (141.7, C 1*s* line at 285.0 eV) [19]. So, the chemical shift of the Gd 4*d* level seems to be strong even among the oxides. Removal of the carbon contaminated layer results in a great increase of the photoemission yield from the constituent element core levels, and new spectral features arise in the spectrum recorded for the clean surface. The wide line at ∼170 eV is also related to Gd 4*d* multiplet and is supposed to be an energy loss peak [19–21]. With surface cleaning the intensity of this line grows proportionally to the intensity of Gd 4*d* component at ∼142 eV. The weak band at ∼122 eV shown in the inset seems to be generated by the Nd 4*d* core level [18,19].

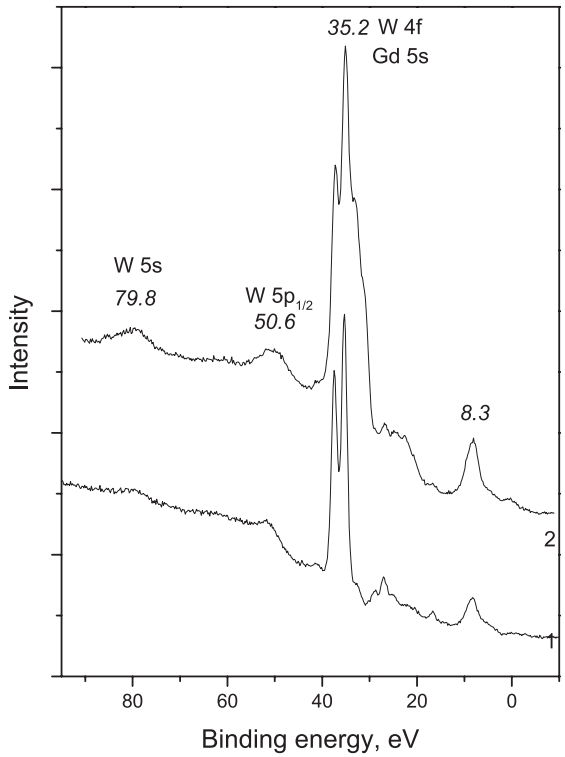

Fig. 5. Valence band spectra for (1) initial and (2) bombarded surfaces.

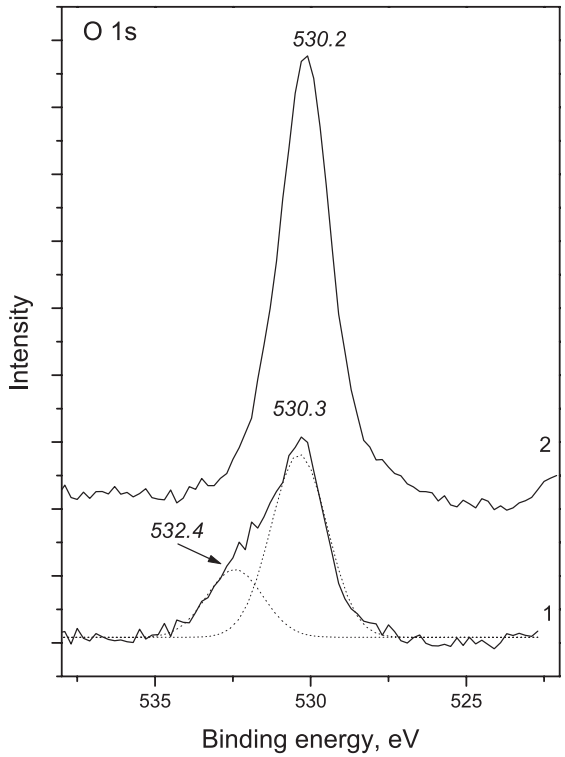

Fig. 6. Detailed spectra of O 1*s* core level for (1) initial and (2) bombarded surfaces.

In Figure 5 the spectra of valence band and adjacent W 5*p* and W 5*s* core levels are shown. The structure of the Nd:KGW valence band is very different for initial and bombarded surfaces. The most intense spectral feature with a maximum at 8.3 eV is present in both spectra and is essentially a combined effect of photoemission from O 2*p* and Gd 4*f* core levels [14,17–21]. For the bombarded surface a weak but pronounced peak appears at ∼2 eV. In tungsten containing oxides the presence of this feature was earlier detected for WO_3 after argon ion bombardment [14], WO_x oxides with $2 \leq x < 3$ [15,16], WO_3 films reduced by annealing [22] and was attributed to photoemission from W 5*d* core level. This core level is empty for the W^{6+} state but partly filled for tungsten ions in lower valence states. So, the appearance of this peak in the spectrum of bombarded Nd:KGW surface confirms oxygen loss accompanied with the formation of lower valence states for the tungsten ion in the modified layer. Further, in the valence band spectrum for the initial surface, a well defined peak at 17 eV is found. After the bombardment this peak spreads into a shoulder at the same binding energy position. This spectral feature was previously detected in valence band spectra of pure KGW crystal surfaces [23] but was not found in valence band spectra of Gd- and W-containing oxides known to us. The line with appropriate binding energy 19.1 eV was reported for Nd-containing oxides $Nd(OH)_3$ [18] and $NdNbO_4$ [19,20]. The Nd content in our crystal is, however, not above few atomic percent and so low doping level excludes the attribution of 17 eV peak to the photoemission from Nd 5*p* core level. Thus, the nature of spectral feature at 17 eV in KGW remains uncertain. At higher binding energies, in the range 20–30 eV, a very complex superposition is observed of Gd 5*p* multiplet with O 2*s* core level [14–16,18–22]. As a result of bombardment, the spectral components of the band were strongly redistributed. A sharp W 4*f* doublet with superimposed Nd 5*s* line is positioned in the energy range 35–40 eV. Low intensity Gd 5*s* line is attached to the higher binding energy side of the W $4f_{5/2}$ component. The bombardment of the surface induces some spreading of both W $4f_{5/2}$ and W $4f_{7/2}$ components and formation of a shoulder on the lower binding energy wing of the doublet. This shoulder indicates the generation of tungsten ions in oxidation states lower than 6+ [14–16,22,24].

The detailed spectra of O 1*s* core level are shown in Figure 6. The peak recorded for the initial surface was essentially asymmetric with a strong shoulder from the higher binding energy side. Fitting of the O 1*s* band reveals the presence of two components with maxima at 530.3 eV and 532.4 eV and intensity ratio (3.1:1.1). The intense component at 530.3 eV is attributed to Nd:KGW and weak component at 532.4 eV seems to be generated by C–O species present in the contaminated top surface layer [13]. After surface cleaning by bombardment the higher binding energy component disappears and only the narrow and symmetric O 1*s* line has been observed.

Relative Nd content in the crystal was low and only the most intense Nd 3*d* core level was suitable for photoemission peak observation. The hydrocarbons present at the initial surface generate a strong C KLL Auger band that makes the Nd $3d_{5/2}$ line undetectable. The detailed spectrum of the Nd $3d_{5/2}$ line recorded for the bombarded

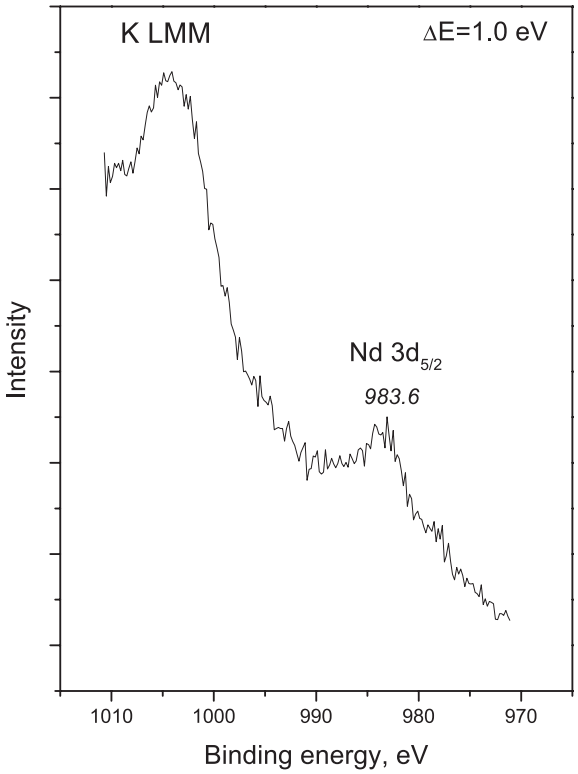

Fig. 7. Detailed spectrum of Nd $3d_{5/2}$ core level for bombarded surface. This core level is recorded with $\Delta E = 1$ eV.

Table 1. Relative element contents at the Nd:KGW surface.

Surface	Element				
	O	K	W	Gd	Nd
Initial	0.62	0.07	0.18	0.11	–
Sputtered	0.56	0.05	0.17	0.133	0.007

surface is presented in Figure 7. To accumulate the photoelectrons emitted from Nd $3d_{5/2}$ level for real time, the energy resolution was changed to $\Delta E = 1.0$ eV. The binding energy of the Nd $3d_{5/2}$ line in Nd:KGW compares well with those determined earlier for several Nd containing oxides [18–20]. It is interesting that the feature at ∼979 eV distinct in spectrum in Figure 7 was reported previously for $NdNbO_4$ [19,20] but absent for $Nd(OH)_3$ [18].

The relative element contents, excluding carbon, at the initial surface and the surface bombarded for 165 min were calculated on the basis of K $2p$, Gd $4d$, W $4f$, O $1s$ and Nd $3d_{5/2}$ peak areas with using relative element sensitivities tabulated in reference [25]. The results presented in Table 1 show reasonable correlation between basic element ratios at the initial surface and nominal KGW composition. The noticeable difference in Gd content seems to be due to the strong variation of relative sensitivity possible for this element in different compounds. Surface sputtering results in some loss of oxygen and potassium. For the bombarded surface, the element content ratio Nd/Gd was estimated as ∼0.05.

The RHEED observation produced just after extraction of the sample from the XPS chamber shows the presence of only amorphous material on the surface. The morphology of the surface is presented in Figure 8. The rms of the surface is ∼2 Å, typical for mechanically polished surfaces. Some linear structures visible in the image are residues of the scratches induced by abrasive grains. So, Nd doping of KGW has not induced pronounced inhomogeneities in the crystal and ion sputtering of the surface proceeds very uniformly. Seemingly, the Ar ion bombardment applied previously for surface cleaning of silica and $CsLiB_6O_{10}$ in references [26,27] can also be used for Nd:KGW surface etching without loss of optical quality.

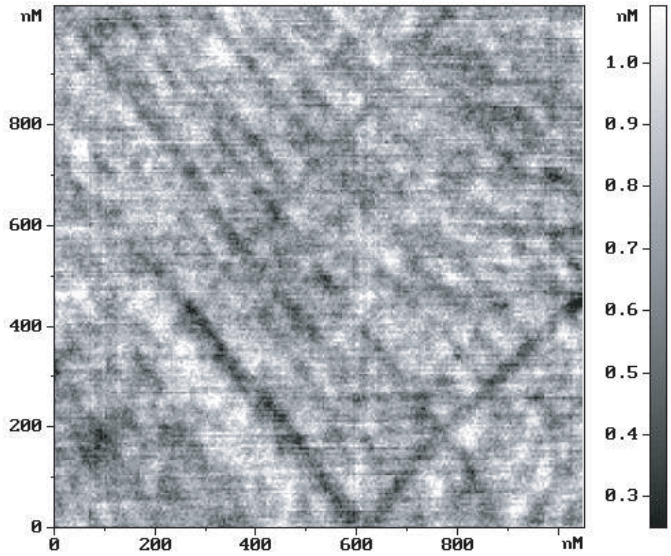

Fig. 8. AFM image of sputtered Nd:KGW surface.

4 Discussion

The complete sets of binding energies of spectral features revealed in the XPS spectra of the initial and bombarded Nd:KGW surfaces are presented in Table 2. For comparison, the binding energies available for representative core levels in tungstates and Gd or Nd containing oxides are shown in Tables 3–5. Regrettably, an analysis of absolute values of the binding energies is complicated by possible differences in the energy scale calibration method [42]. In many publications, moreover, the calibration method was not even reported. In this situation, using energy difference between metal and O $1s$ core levels is reasonable as an additive criterion independent of the energy reference line. Improved robustness of the method was demonstrated earlier for many complex dielectric oxides [12,23,43–46]. So, Tables 2–4 are completed with the parameters, when available, necessary for calculation of binding energy differences.

The collection of XPS results for tungstates is sufficiently representative to test the scattering ranges of the binding energies of characteristic element lines. Let us consider only the reports in which both O $1s$ and W $4f_{7/2}$ core levels are found in one study and in the same energy scale calibration. Further, it is reasonable to exclude the

Table 2. Binding energies of element core levels of the Nd:$KGd(WO_4)_2$ surface.

Binding energy, eV		Core level
Initial surface	Bombarded surface	
35.2	35.2	W $4f_{7/2}$*, Gd $5s$
51.3	50.6	W $5p_{1/2}$
79.8	79.8	W $5s$
142.4	142.2	Gd $4d_{5/2}$
147.6	147.5	Gd $4d_{3/2}$
170.0	170.0	Gd $4d$ satelite
247.2	246.4	W $4d_{5/2}$
259.8	259.1	W $4d_{3/2}$
–	271.4	Gd $4p_{3/2}$
284.6	–	C$1s$**
292.4	292.3	K $2p_{3/2}$
295.2	–	K $2p_{1/2}$
360–400	360–400	Gd MNN, Gd $4s$
427.0	425.3	W $4p_{3/2}$
530.3	530.2	O $1s$
742.1	741.6	O KLL
763.2	761.7	O KLL
993.6	–	C KLL
–	983.6	Nd $3d_{5/2}$
–	1003.6	K LMM
1013.7	–	?
–	1085.0–1144.5	W, Gd Auger
–	1187.6	Gd $3d$

* Used for binding energy scale calibration for bombarded surface; ** used for binding energy scale calibration for initial surface.

Table 3. Binding energies of representative core levels in tungstates.

Compound	Binding energy, eV			Reference
	O $1s$	W $4f_{7/2}$	O $1s$–W$4f_{7/2}$	
WO_2		33.05		32
m-WO_3	530.5	35.67	494.83	15
h-WO_3	530.86	36.02	494.84	16
WO_3	530.4	35.6	494.8	13
WO_3	530.5	35.5	495.0	28
WO_3		35.8		22
WO_3		36.1		24
WO_3		36.0		42
Li_2WO_4	530.7	35.6	495.1	13
Na_2WO_4	530.6	35.3	495.3	13
Na_2WO_4	530.2			30
$KGd(WO_4)_2$	530.1	35.2	494.9	23
Ag_2WO_4	530.3	35.2	495.1	13
$(NH_4)_2WO_4$	530.4	35.5	494.9	13
$CaWO_4$	530.1	35.1	495.0	29
$Al_2(WO_4)_3$	531.8	35.4	496.4	31
$NiWO_4$	531.5	35.2	496.3	31

Table 4. Binding energies of representative core levels in Gd containing oxides.

Compound	Binding energy, eV					Reference
	O $1s$	Gd $4d_{5/2}$	Gd $3d_{5/2}$	O $1s$–Gd $4d_{5/2}$	Gd $3d_{5/2}$–O $1s$	
Gd_2O_3	531.2	142.5	1187.6	388.7	656.4	17
Gd_2O_3	530.8	142.8		388.0		33
$Gd(OH)_3$		141.17	1187.46			18
$Gd(OH)_3$			1186.8			34
$GdNbO_4$		141.7	1186.7			19,20
$KGd(WO_4)_2$	530.1	142.3	1187.6	387.8	657,5	23
$Gd_2Ti_2O_7$	∼529.5		1187.2		657.7	35
$Gd_2Zr_2O_7$	∼529.4		1186.7		657.3	35

Table 5. Binding energies of representative core levels in Nd containing oxides.

Compound	Binding energy, eV				Reference
	O 1s	Nd 4d	Nd 3$d_{5/2}$	Nd 3$d_{5/2}$–O 1s	
Nd_2O_3			981.4		37
Nd_2O_3			981.7		38
$Nd(OH)_3$		121.30	980.77		18
$Nd(OH)_3$			981.7		34
Nd_2CuO_4	528.4		981.4	453.0	37
$NdGaO_3$	529.8		981.4	451.6	39
$NdGaO_3$	528.14		980.48	452.34	40
$NdNbO_4$		121.5	982.6		19, 20
$Li_{0.30}Nd_{0.57}TiO_3$	529.8		982.6	452.8	41
$CaNdAlO_4$	529.08		981.19	452.11	40
$Nd_{1.85}Ce_{0.15}CuO_4$	528.6		981.4	452.8	37
$Nd_{1.85}Ce_{0.15}CuO_4$	529.5		982	452.5	36

results of reference [28], in which the binding energy of O 1s level was evidently overestimated. After this the scatter in binding energy values of the O 1s core level is 0.8 eV and the scatter for the W 4$f_{7/2}$ core level is 0.9 eV. Comparatively, the dispersion of the (O 1s–W 4$f_{7/2}$) difference is only 0.5 eV. For Nd:KGW, the values of the binding energies of O 1s and W 4$f_{7/2}$ core levels evaluated for the initial surface are in the ranges typical for dielectric tungstates with W^{6+} ions. The relevant energy difference (O 1s–W 4$f_{7/2}$) also lies in the range characteristic for oxides with W in the 6+ oxidation state. The shoulder appearing from the lower energy side of W 4$f_{7/2}$ line after bombardment is in good agreement with the energy positions reported for W^{4+} ions in WO_2 and W^{2+} [32]. The oxides with tungsten in these oxidation states are conductive, and therefore bombarded KGW surfaces should also possess higher conductivity and, respectively, greatly lower optical damage threshold than that of the initial dielectric surface.

Although the collection of XPS results for Gd core levels in different oxides is very limited, the energy positions of O 1s and Gd lines defined for the initial surface are evidently within the values measured earlier for different Gd^{3+} containing oxides. The energy difference (O 1s–Gd 4$d_{5/2}$) is practically the same for initial and clean Nd:KGW surfaces that confirms keeping of oxygen chemical environment around Gd^{3+} ions on bombardment. Among the photoemission lines of the neodymium ion, only the most intensive Nd 3$d_{5/2}$ peak is sufficiently strong to define the binding energy of the core level for the cleaned Nd:KGW surface. The binding energy of the maximum and the energy difference (Nd 3$d_{5/2}$–O 1s) relate well with the values reported earlier for several Nd containing oxides.

5 Conclusions

The electronic and surface structural properties of Nd:KGW are very similar to those of pure KGW [23]. As is already known, neodymium ions substitute isomorphously for gadolinium in the $KGd(WO_4)_2$ crystal lattice [1,47]. The radii of Nd^{3+} and Gd^{3+} ions are very close and at low doping level there is no strong impact on the interatomic distances between metal and oxygen ions in the KGW crystal lattice. For this reason the Nd incorporation induces only negligible chemical shifts in the binding energies of K, Gd and W core levels, and the electronic spectra of the crystal remain nearly the same besides features related to Nd core levels.

The bombardment of the Nd:KGW surface with middle energy Ar ions generates drastic variations in K and W core levels with the formation of lower valence states of tungsten. However, there are no variations in the Gd core levels, indicating enhanced stability of the oxygen environment around this cation. In any case, the bombardment of Nd:KGW crystal surface with Ar ions, 3 keV, 2.75 h, results in complete amorphization of the surface. It seems likely that annealing at an appropriate temperature in an oxygen atmosphere would be a reasonable way to restore the crystalline state of the surface. Thus, ion bombardment may be used for top surface cleaning of polished Nd:KGW surface, but further observation of sputtering effects and determination of a temperature interval optimal for surface restructurization would be useful.

References

1. M.C. Pujol, R. Solé, Jna. Gavaldà, J. Massons, M. Aguiló, F. Díaz, J. Mater. Res. **14** (9), 3739 (1999)
2. A.A. Kaminskii, A.A. Pavlyuk, P.V. Klevtsov, I.F. Balashov, V.A. Berenberg, S.E. Sarkisov, V.A. Fedorov, M.A. Petrov, V.V. Lyubchenko, Izv. Acad. Nauk SSSR, Neorg. Mater. **13** (3), 582 (1977)
3. V. Kushawaha, L. Major, Optics Laser Technol. **26** (5), 351 (1994)
4. I.V. Mochalov, J. Opt. Technol. **62**, 746 (1995)
5. R. Moncorgé, B. Chambon, J.Y. Rivoire, N. Garnier, E. Descroix, P. Laporte, H. Guillet, S. Roy, J. Mareschal, D. Pelenc, J. Doury, P. Farge, Opt. Mat. **8**, 109 (1997)
6. A.S. Grabtchikov, A.N. Kuzmin, V.A. Lisinetskii, G.I. Ryabtsev, V.A. Orlovich, A.A. Demidivich, J. Alloys Comp. **300–301**, 300 (2000)
7. P. Černy, H. Jelínkova, P.G. Zverev, T.T. Basiev, Prog. Quant. Elect. **28**, 113 (2004)
8. P.A. Atanasov, R.I. Tomov, J. Perriére, R.W. Eason, N. Vainos, A. Klini, A. Zherikhin, E. Millon, Appl. Phys. Lett. **76** (18), 2490 (2000)

9. P.A. Atanasov, M. Jiménez de Castro, A. Perea, J. Perrière, J. Gonzalo, C.N. Afonso, Appl. Surf. Sci. **186**, 469 (2002)
10. P.A. Atanasov, T. Okato, R.I. Tomov, M. Obara, Thin Solid Films **453–454**, 150 (2004)
11. Feng Chen, Hui Hu, Ke-Ming Wang, Zhen-Xiang Cheng, Huan-Chu Chen, Qing-Ming Lu, Ding-Yu Shen, Appl. Surf. Sci. **181**, 145 (2001)
12. V.V. Atuchin, V.G. Kesler, N.Yu. Maklakova, L.D. Pokrovsky, V.N. Semenenko, Surf. Interface Analysis **34**, 320 (2002)
13. S.F. Ho, S. Contarini, J.W. Rabalais, J. Phys. Chem. **91**, 4779 (1987)
14. R.A. Dixon, J.J. Williams, D. Morris, J. Rebane, F.H. Jones, R.G. Egdell, S.W. Downes, Surf. Sci. **399**, 199 (1998)
15. O.Yu. Khyzhun, J. Alloys Comp. **305**, 1 (2000)
16. Yu.M. Solomin, O.Yu. Khyzhun, E.A. Graivoronskaya, Cryst. Growth Design **1** (6), 473 (2001)
17. D. Raiser, J.P. Deville, J. Elect. Spect. Rel. Phenom. **57**, 91 (1991)
18. D.F. Mullica, C.K.C. Lok, H.O. Perkins, G.A. Benesh, V. Young, J. Elect. Spect. Rel. Phenom. **71**, 1 (1995)
19. Yu.A. Teterin, T.N. Bondarenko, A.Yu. Teterin, A.M. Lebedev, I.O. Utkin, Radiochemistry **40** (2), 107 (1998)
20. Yu.A. Teterin, T.N. Bondarenko, A.Yu. Teterin, A.M. Lebedev, I.O. Utkin, J. Elect. Spect. Rel. Phenom. **96**, 221 (1998)
21. J. Szade, M. Neumann, I. Karla, B. Schneider, F. Fangmeyer, M. Matteucci, Solid State Comm. **113**, 709 (2000)
22. S. Santucci, C. Cantalini, M. Crivellari, L. Lozzi, L. Ottaviano, M. Passacantando, J. Vac. Sci. Technol. A **18** (4), 1077 (2000)
23. V.V. Atuchin, V.G. Kesler, N.Yu. Maklakova, L.D. Pokrovsky, Solid State Commun. **133**, 347 (2005)
24. J. Haber, J. Stoch, L. Ungier, J. Solid State Chem. **19**, 113 (1976)
25. D. Briggs, M.P. Seah, *Practical Surface Analysis*, 2nd edn. (John Wiley, Chichester, 1995), Vol. 1
26. Tomosumi Kamimura, Yusuke Mori, Takatomo Sasaki, Hidetsugu Yoshida, Takayuki Okamoto, Kunio Yoshida, Jpn J. Appl. Phys. **37** (9A), 4840 (1998)
27. Takatomo Sasaki, Yusuke Mori, Masashi Yoshimura, Yoke Knin Yap, Tomosumi Kamimura, Mater. Sci. Eng. **30**, 1 (2000)
28. T.H. Fleisch, G.J. Mains, J. Chem. Phys. **76** (2), 780 (1982)
29. V.I. Nefedov, J. Elect. Spect. Rel. Phenom. **25** (1), 29 (1982)
30. C.D. Wagner, D.A. Zatko, R.H. Raymond, Anal. Chem. **52** (9), 1445 (1980)
31. K.T. Ng, D.M. Hercules, J. Phys. Chem. **80** (19), 2094 (1976)
32. F.J. Himpsel, J.F. Morar, F.R. McFeely, R.A. Pollak, Phys. Rev. **30** (12), 7236 (1984)
33. J.A. Gupta, D. Landheer, G.I. Sproule, J.P. McCaffrey, M.J. Graham, K.-C. Yang, Z.-H. Lu, W.N. Lennard, Appl. Surf. Science **173**, 318 (2001)
34. K. Tatsumi, M. Tsutsui, G.W. Beall, D.F. Mullica, W.O. Milligan, J. Elect. Spect. Rel. Phenom. **16** (1), 113 (1979)
35. J.M. Sohn, M.R. Kim, S.I. Woo, Cat. Today **83**, 289 (2003)
36. H. Yamamoto, M. Naito, H. Sato, Physica C **291**, 67 (1997)
37. T. Suzuki, M. Nagoshi, Y. Fukuda, K. Oh-ishi, Y. Syono, M. Tachiki, Phys. Rev. **42** (7), 4263 (1990)
38. Chikashi Suzuki, Jun Kawai, Masao Takahashi, Aurel-Mihai Vlaicu, Hirohiko Adachi, Takeshi Mukoyama, Chem. Phys. **253**, 27 (2000)
39. E. Talik, M. Kruczek, H. Sakowska, Z. Ujma, M. Gala, M. Neumann, J. Alloys Comp. **377**, 259 (2004)
40. A. Novosselov, E. Talik, A. Pajaczkowska, J. Alloys Comp. **351**, 50 (2003)
41. Q.N. Pham, C. Bohnke, O. Bohnke, Surf. Sci. **572**, 375 (2004)
42. P. Swift, Surf. Interface Analysis **4** (2), 47 (1982)
43. Y. Fukuda, M. Nagoshi, T. Suzuki, Y. Namba, Y. Syono, M. Tachiki, Phys. Rev. **39** (16), 11494 (1989)
44. V.V. Atuchin, L.D. Pokrovsky, V.G. Kesler, L.I. Isaenko, L.I. Gubenko, J. Ceram. Proc. Res. **4** (2), 84 (2003)
45. L. O'Mahony, T. Curtin, D. Zemlyanov, M. Mihov, B.K. Hodnett, J. Cat. **227**, 270 (2004)
46. V.V. Atuchin, I.E. Kalabin, V.G. Kesler, N.V. Pervukhina, J. Elect. Spect. Rel. Phenom. **142**, 129 (2005)
47. P.V. Klevtsov, R.F. Klevtsova, J. Struct. Chem. **18** (3), 419 (1977)